3D Bioprinting of a Complex Skin Construct Using the BIO X6 Bioprinter

Elahe Hadavi, PhD; Itedale Namro Redwan, PhD
Gothenburg, Sweden

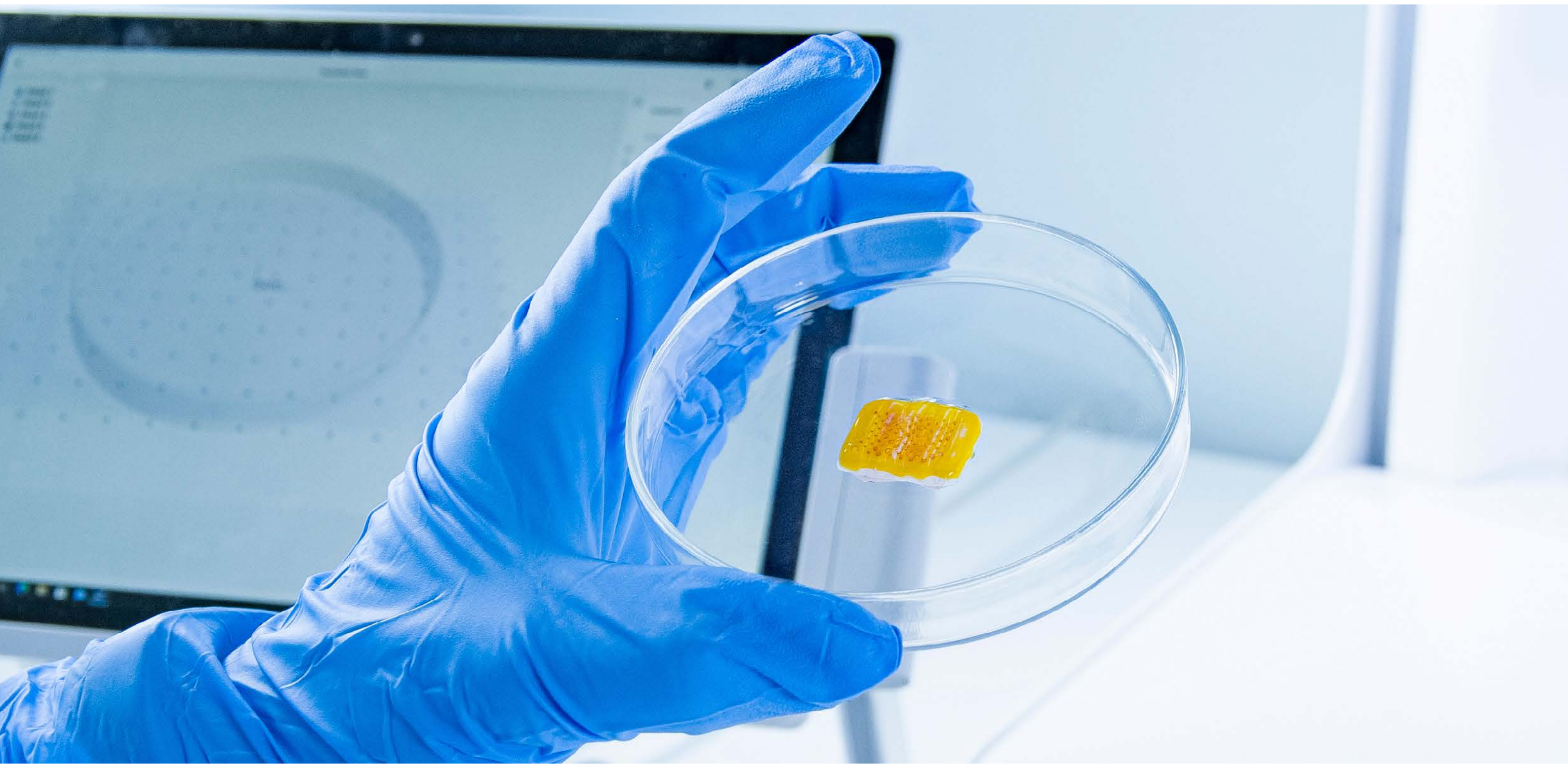

Abstract

The native skin is a complex tissue consisting of three main layers: the epidermis, dermis and hypodermis. To date, significant progress has been made in the development of skin models using tissue-engineering techniques. Despite the advancement in fabrication of skin constructs for clinical applications, there is a major limitation in biofabrication of a full-skin equivalent construct. Here, we have designed and 3D bioprinted a complex hierarchical skin construct using CELLINK's BIO X6™ bioprinter. The multilayered 3D skin construct consists of a hypodermis layer containing adipocytes and blood vessels, a dermis layer containing fibroblasts, hair follicles and capillaries, and an epidermis layer containing melanocytes. The three layers were bioprinted using CELLINK bioinks GelMA FIBRIN and GelXA FIBRIN and various cell types. The BIO X6 bioprinter's advanced and automated platform, with its six different printheads and photocrosslinking modules, facilitated the 3D bioprinting of the complex structure. The viability of the cells and morphology of the 3D bioprinted construct was evaluated by histology staining and live/dead assay. The results indicate good cell viability and well-defined 3D structures with sufficient printing accuracy for the 3D bioprinted skin constructs over 14 days, resembling native skin tissue.

Introduction

Skin is the largest organ of the body and plays a critical role in protection, thermoregulation, sensation and communication between the external environment and the inner organism (Brohem, 2011). Fulfilling these varied functions requires a complex anatomy that includes the epidermis, dermis and hypodermis layers **(Figure 1A)**. The epidermis is the outer layer of the skin and includes keratinocytes, melanocytes, as well as Merkel and Langerhans cells (Boulais, 2007). The epidermis layer functions as the skin barrier, producing melanosome (pigment for the skin) as well as immunological functions. The middle layer is the dermis, composed of blood vessels, nerve endings and hair follicles, which provide nutrients, sensation and regulation of the body's temperature, respectively. The dermis layer also includes fibroblasts to synthesize cytokines, collagen fibers, elastic fibers, reticular fibers and other extracellular components that promote wound repair, protection and skin elasticity (Starcher, 2005; Douillet, 2022). Beneath the dermis, there is the hypodermis layer that includes adipocytes and collagen (Gilaberte, 2016). The dermis is responsible for the storage of energy, thermoregulation and connecting the dermis layer to muscles and bones. It can also buffer deep tissues from severe trauma, provide buoyancy and even function as an endocrine organ (Weng, 2021).

The rapid closure and early treatment of acute and chronic wounds is critical for normal healing and avoiding hypertrophic and keloid scars (Martin, 2015). Hypertrophic and keloid scars are known as fibroproliferative outgrowth beyond the boundaries of the original wound margin as well as abnormal deposits of collagen within a wound (Gauglitz, 2011). Despite the high regeneration ability of the skin, large-scale deep injuries cannot always be completely repaired (Thompson, 2013) and can result in an insufficient regeneration of hair follicles and sweat glands. This abnormality of skin may impair prognosis and quality of life for patients. It affects their personal appearance and may lead to depression. The conventional treatment for skin defects has been autologous skin transplantation (Richters, 2005). However, this technology has its drawbacks, such as finding adequate donor sites, pain, scarring, risks of infection and secondary injuries. Recently, tissue-engineered skin models displayed promising results when treating skin defects, and FDA-approved models, like Integra (Schneider, 2009), StrataGraft (Centanni, 2011), Dermagraft (Marston, 2004) and PELNAC (Widjaja, 2016), are available on the market. The current tissue-engineered skin models can be categorized into three groups: epidermal constructs, dermal constructs, and epidermal-dermal composite constructs (Shevchenko, 2010). These are subclassified as acellular or cellular-based composition (Daikuara, 2021). Despite advances in skin tissue-engineering techniques, the therapeutic opportunities for full-thickness skin repair are limited (Daikuara, 2021; Huber, 2016). Currently, there is a need to bioengineer full-thickness skin equivalent constructs composed of hypodermis, dermis, epidermis, pigmentation, elasticity, hair follicles, vascular networks and other skin appendages specific to each patient.

Using 3D bioprinting techniques offers many advantages over traditional tissue-engineering techniques. Advances in 3D scanning and computer-aided design have helped researchers design personalized skin grafts based on the size, shape and depth of the wounds (Li, 2017). 3D bioprinting also enables a precise fabrication process with accurate specifications (Miri, 2019). The technology offers flexibility in using various types of biomaterials, cells, nucleic acids and growth factors for fabrication of a biomimetic skin construct. 3D bioprinting makes it possible to control the created tissue's stiffness, elasticity, texture, porosity, pigmentation and morphology, which are important factors for successful cell adhesion, viability, function, as well as the exchange of gas and nutrients (Javaid, 2021). In addition to advancing the treatment of skin defects, 3D bioprinted skin models can pave the way for disease modeling, understanding of pathological mechanisms, as well as testing the efficiency and toxicity of drugs (Gao, 2021).

In this study, we have designed a complex hierarchical skin model consisting of epidermis, dermis, hypodermis, blood vessels and hair follicles. The construct was 3D bioprinted using the BIO X6 bioprinter. The bioprinter is compatible with a range of printheads that enable the precise control of design, structure, mechanical properties and depositing of the cells. Using a 3D bioprinter eliminates the need to use separate planar containers for crosslinking an engineered construct. The BIO X6 also boasts coaxial bioprinting capabilities to facilitate the printing of vasculature channels, which are currently fundamentally challenging in tissue engineering. This study presents a suggested workflow for the fabrication of a biomimetic full-skin equivalent.

Materials and methods

CELL PREPARATION

Cell culture

The human dermal fibroblast cells (HDF, AvantiCell, DF-HN-184), human umbilical vein endothelial cells (HUVECs, ATCC, CRL-4053), human follicle dermal papilla cells (HFDPCs, PromoCell, 190917), and melanocytes (CELLnTECH, HEMns) were cultured in fibroblast growth medium 2 (PromoCell), EGM-2 endothelial cell growth medium-2 (Lonza, CC-3162-6), follicle dermal papilla cell growth medium (PromoCell, 23020), CnT-40 melanocyte proliferation medium (CELLnTEC, CnT-40), respectively. All cell types were grown under standard culture conditions, at 37°C in 5% CO_2.

Adiposity differentiation

Human-derived adipose mesenchymal stem cells (hAD-MSCs, PromoCell, 20190701) were cultured in Dulbecco's Modified Eagle's Medium (DMEM) low glucose (Fisher Scientific, 11570586) (1 g/L) supplemented with 10% fetal bovine serum (FBS, Gibco, 10270-106) and 1% penicillin/streptomycin (Fisher Scientific, 15140-122). To induce adipocyte differentiation and reach pre-adipocyte state **(Figure 3H)**, cells were cultured in DMEM/F12 (Fisher Scientific, 11320033) supplemented with 10% FBS, 1% penicillin/streptomycin, 5 µg/mL insulin (Sigma-Aldrich, I9278), 1 nM of 3,3',5'-triiodo-L-thyronine (T_3, Sigma-Aldrich, T6397), 2 µg/mL of dexamethasone (Sigma-Aldrich, D1756-25MG), and 0.5 mM of isobutyl-1-methylxanthine (IBMX, Sigma-Aldrich, I5879-100MG) for 6 days. Afterward the adipocyte maturation process continued in the bioprinted construct using the universal culture medium (see details below), which was optimized to fulfill the requirements of different cell types in the construct **(Figure 3D, E, F, I)**.

Universal culture medium for the bioprinted skin construct

Universal culture medium for the bioprinted construct was composed of 50% DMEM/F12 (Fisher Scientific, 11320033) and 50% EGM-2 basal medium (Lonza, CC-4176). The medium was supplemented with 5 µg/mL of insulin, 1 µM Rosiglitazone (Sigma-Aldrich, R2408), 2 µg/mL of dexamethasone, 10 µM Forskolin (Sigma-Aldrich, F6886), 1 nM of T_3, and 2% FBS. Moreover, all supplements of EGM-2 SingleQuots Supplement Kit (Lonza, CC-3162-6), except human epidermal growth factor (hEGF) and hydrocortisone supplements, were added according to the manufacturer's instructions, equivalent to the total volume of the universal culture medium. The total volume of 500 mL universal culture medium was supplemented with 3 mL human basic fibroblast growth factor (hFGF-B), 0.50 mL VEGF, 0.50 mL R3-IGF-1, 0.50 mL ascorbic acid, 0.50 mL GA-1000 and 0.50 mL heparin.

BIOPRINTING PROCESS

Bioprinter

The BIO X6 bioprinter (CELLINK, S 10002-001) was used to develop a biomimetic full-skin construct based on the anatomy of native skin **(Figure 1)**. The BIO X6 bioprinter is an advanced and user-friendly extrusion-based bioprinter, and its wide range of compatible printhead accessories offer precise control of temperature, motion, extrusion rate, volume and printing resolution of different types of bioinks, with or without cells. In addition, the BIO X6 is equipped with four built-in photocuring modules as well as toolheads that allow photocrosslinking of bioinks at different wavelengths (365 nm, 405 nm, 485 nm and 520 nm). For this study, the Pneumatic Printhead (CELLINK, 000000020340), Temperature-controlled Printhead (CELLINK, 000000020346), Syringe Pump Printhead (CELLINK, 000000020855), Electromagnetic Droplet (EMD) Printhead (CELLINK, 000000020566) and a coaxial kit (CELLINK, D16110023750) were used **(Figure 1D)**. The Pneumatic Printhead leverages pneumatic pressure to extrude the bioink, and the temperature can be set up to 65°C. The Temperature-controlled Printhead provides a high range of flexibility in cooling down and heating up from about 4°C (~17°C below ambient temperature) to 65°C. The Syringe Pump Printhead allows superior control of bioink extrusion process by defining flow rate, speed and deposited volume. The EMD Printhead is an inkjet technology that is equipped with a piezoelectric valve and is ideal for spraying, droplet generation and micropatterning. The coaxial bioprinting kit simultaneously deposits two bioinks in a single filament, in a concentric structure where one bioink is printed as the core and the other as a shell around the core. The coaxial setup facilitates the fabrication of hollow, solid and multilayered filaments with or without cells. To provide a sterile working environment, the BIO X6 was placed in a biosafety cabinet and sterilized using the bioprinter's built-in UV-C feature. The bioprinting condition for different tissue layers of the complex skin are mentioned in the next paragraph.

Hypodermis

The GelMA FIBRIN (CELLINK, IKG106L3030-M) was mixed with pre-adipocyte cells at a density of 5 x 10^6 cells/mL bioink and transferred to a cartridge. The cartridge was loaded into the Temperature-controlled Printhead at slot 3 and capped with a 22G nozzle (CELLINK, NZ4220005001) **(Figure 1D, E)**. The bioprinting settings were printhead temperature of 29°C, pressure of 55 kPa, and print speed of 3 mm/s. Moreover, the printbed temperature was adjusted to 18°C.

Dermis

GelXA FIBRIN (CELLINK, IK3X21390301) was laden with the co-culture of HDFs and HUVECs at a density of 1 x 10^6 and 3 x 10^6 cells/mL bioink, respectively. The cartridge was loaded into the Temperature-controlled Printhead at slot 4 and capped with a 22G nozzle **(Figure 1D, F)**. The bioprinting settings were adjusted to a temperature of 23°C, pressure of 55 kPa, and print speed of 5 mm/s.

Blood vessels

GelXA bioink was mixed with HUVECs at a density of 8 x 10^6 cells/mL and printed as the outer layer in the dispensing coaxial system. 30% Pluronics (CELLINK, IKS400000503) was used as the inner layer bioink. The cartridges for the inner and outer layers were loaded into the Pneumatic Printheads located at slots 1 and 2, respectively. The coaxial nozzle (CELLINK, D16110023750) with the size of 18G-14G and 0.5 inch length was connected to the cartridges loaded in slots 1 and 2 **(Figure 1D, F)**. The bioprinting settings were adjusted to inner nozzle pressure of 120 kPa, outer nozzle pressure of 55 kPa, print speed of 3 mm/s, and temperature of 30°C.

Hair follicles

The custom-made 2.5% GelMA FIBRIN was laden with HFDPCs at a density of 7 x 10^6 cells/mL bioink. The related cartridge was assembled on the Syringe Pump Printhead at slot 5 and capped with a 22G needle (CELLINK, KT0000002002) **(Figure 1D, I)**. The bioprinting settings were adjusted to an extrusion rate of 3 μL/s, extrusion volume of 3 μL, and print speed of 1 mm/s.

Epidermis

The custom-made 2.5% GelMA FIBRIN - LAMININ 521 with a high concentration of fibrinogen was mixed with melanocytes at a density of 7 x 10^6 cells/mL bioink. A cartridge with the bioink was loaded into the EMD Printhead, enabling the contactless jetting and spraying of the cells on the surface of the skin construct **(Figure 1D, J)**. The bioprinting settings were adjusted to a pressure of 6 kPa, 2 mm/s print speed, 9 ms open time, 30 ms cycle time, and temperature of 30°C.

Crosslinking

The construct was crosslinked for 15 seconds at layers 3, 4, 7 and 8 with the 405 nm wavelength (module 2), intensity of 100%, the height of 6 cm above the center of the layer surface **(Figure 1G)**. The chamber light was off during the bioprinting process due to the presence of photosensitive bioinks.

Post-bioprinting condition

To create fibrin network in the skin constructs after bioprinting, the bioprinted construct was immersed in the universal culture medium supplemented with 10 U/mL thrombin and kept there overnight. Subsequently, the universal culture medium (without thrombin) was replaced with the maximum working volume of each well, every 2 days (2 mL per well in a 6-well plate).

Analysis

Samples were collected at days 4, 7 and 14 and fixed for histology staining in 4% paraformaldehyde (Histolab Products AB, 02176), according to CELLINK's fixation protocol. Subsequently, they were embedded in paraffin and sectioned following CELLINK's protocols. After deparaffinization of the samples, the hematoxylin and eosin (H&E) staining was performed following CELLINK's deparaffinization and H&E staining protocols. Moreover, the immunofluorescence staining using Anti-alpha-Smooth Muscle Actin primary antibody (Thermo Fisher, 14-9760-82) and Goat anti-Mouse IgG (H+L) Highly Cross-Adsorbed secondary antibody (1:50), Alexa Fluor 488 (Thermo Fisher, A-11029) (1:200) and DAPI (Thermo Fisher, P36962) were performed following CELLINK's immunofluorescence-staining protocol. To identify the lipid droplets in differentiated adipocytes, the samples were stained with BODIPY493/503 (Invitrogen, D3922) and DAPI, following the manufacturer's protocol. To determine the viability of cells, the samples (n=3) were collected at days 4, 7 and 14, and live/dead assay was performed following CELLINK's viability protocol. The samples were imaged using the Olympus IX73 microscope. The above-mentioned protocols can be accessed on CELLINK's website.

Results and discussion

A biomimetic full-skin equivalent was 3D bioprinted using CELLINK's BIO X6 bioprinter. The final construct was composed of a hypodermis containing adipocytes and blood vessels bioprinted as tubular hollow fibers, a dermis containing fibroblasts, hair follicles and capillaries formed from dispersed endothelial cells, as well as a simplified epidermis containing melanocytes, similar to the structure illustrated in **Figure 1.**

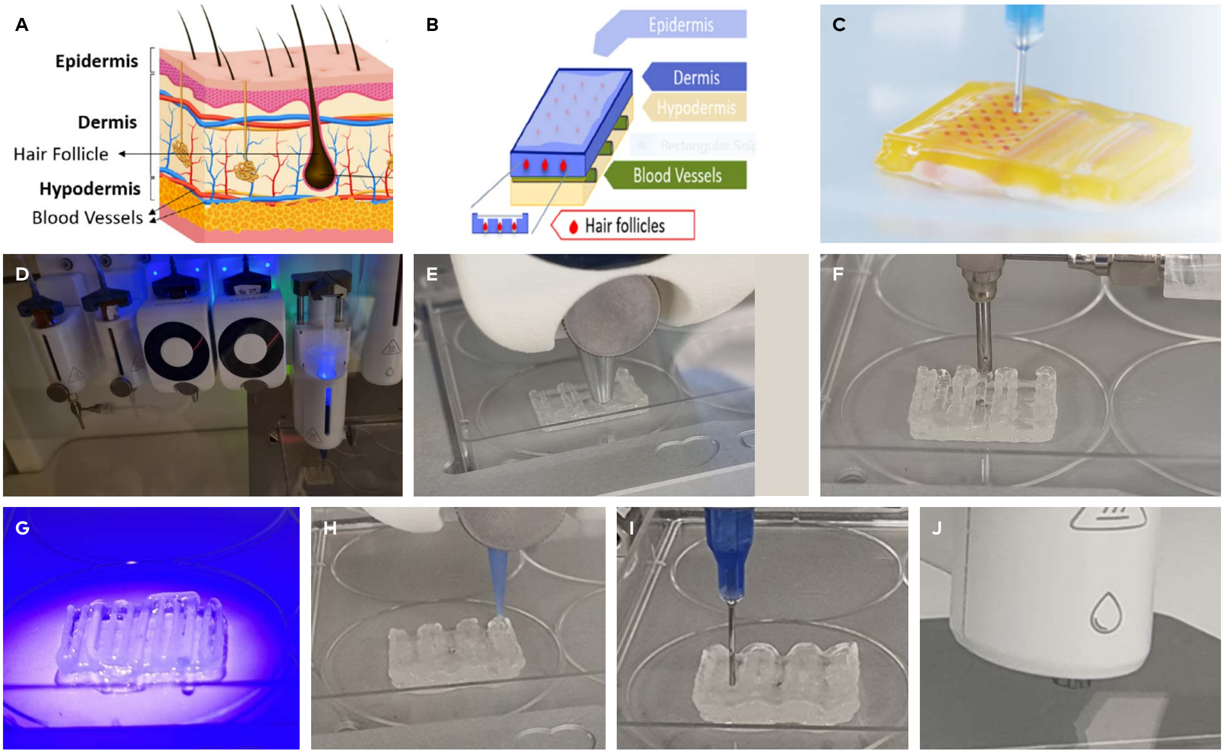

***Figure 1**. Illustration of the 3D bioprinting process of a complex skin construct using the BIO X6 bioprinter. **A)** Anatomy of native skin, **B)** schematic representation of the skin construct design, **C)** 3D construct printed with sacrificial bioinks, **D)** bioprinting setup, including printheads with coaxial nozzles to produce blood vessels (slots 1 and 2), Temperature-controlled Printhead to 3D bioprint the hypodermis layer (slot 3), Temperature-controlled Printhead for 3D bioprinting the dermis layer (slot 4), Syringe Pump Printhead to dispense hair follicles (slot 5), and EMD Printhead for epidermis layer (slot 6), **E)** 3D bioprinting process of the hypodermis, **F)** 3D bioprinting of the vessel, **G)** photo-crosslinking process, **H)** 3D bioprinting of dermis, **I)** depositing of hair follicles and **J)** spraying of epidermis.*

Viability of cells

To evaluate the cell viability and cytocompatibility of the different cell types in all three layers of the 3D bioprinted skin construct, live/dead assay was performed on days 4, 7 and 14 post bioprinting **(Figure 2)**. The live/dead staining revealed a cell viability of >78% for adipocyte cells in the hypodermis layer at days 4, 7 and 14 post bioprinting **(Figure 2A, B, C, M)**. The live/dead staining of co-culture of HUVECs and HDFs in the dermis layer indicated a viability of about 82%, including rounded and stretched cells. At day 7, in addition to cell viability enhancement (89%), the high rate of tubular network formation was observed. Although the rate of tubular network and viability of the cells dropped to 60% at day 14 **(Figure 2D, E, F, M)**, this might be further improved by optimizing the bioprinting and post-bioprinting conditions, such as crosslinking time or volume of medium. The viability of melanocyte cells in the epidermis layer at day 4 was 72%. The viability increased to 80% at day 7 and remained stable up to 14 days **(Figure 2G, H, I, M)**.

The majority of HUVECs in the coaxial bioprinted vessel (bioprinted hollow fiber) were rounded, and the viability was low (59%) at day 4. Along with the enhancement of the stretched HUVECs at day 7, the viability rate also increased to 80%. At day 14, the viability of cells reduced to 60% **(Figure 2J, K, L, M)**. In addition to the high extrusion pressure, the presence of Pluronics bioink, even after washing steps, might have negatively affected the viability of the cells at day 4. In future experiments, optimization of the printhead temperature could help reduce the extrusion pressure for the outer layer. The reduction of the HUVECs viability 14 days post bioprinting—similar to that of the dermis layer—may be improved by optimizing the perfusion cultivation system or medium volume. Plus, optimizing the washing step of the inner layer of the coaxial bioprinted vessel or the application of other more cell-friendly sacrificial bioinks, such as agarose (Ma, 2018), gelatin (Lee, 2014), alginate (Xu, 2015), might further improve the viability and outcome of vessel bioprinting.

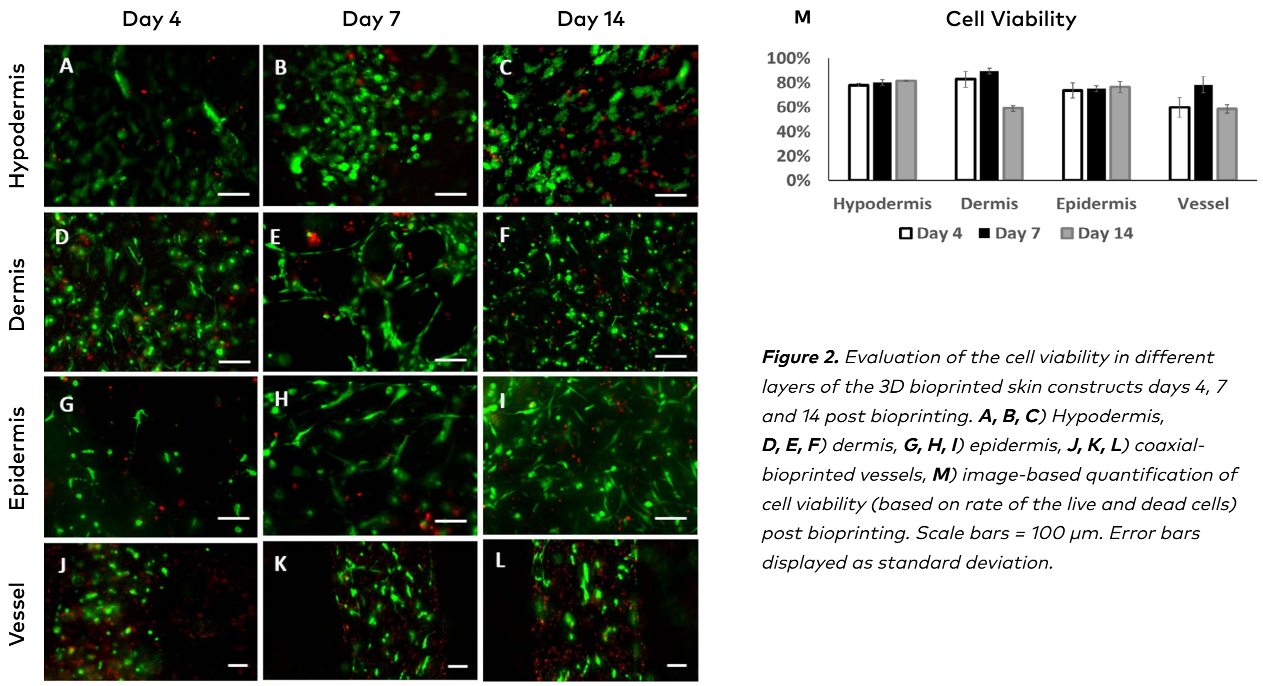

***Figure 2.** Evaluation of the cell viability in different layers of the 3D bioprinted skin constructs days 4, 7 and 14 post bioprinting. **A, B, C**) Hypodermis, **D, E, F**) dermis, **G, H, I**) epidermis, **J, K, L**) coaxial-bioprinted vessels, **M**) image-based quantification of cell viability (based on rate of the live and dead cells) post bioprinting. Scale bars = 100 µm. Error bars displayed as standard deviation.*

Universal culture medium condition to support the various cells

To develop a 3D bioprinted complex tissue or organ, multiple cell types must be included in the biofabricated construct. Therefore, a universal culture medium that includes adequate growth factors and supplements to support the viability, growth and differentiation of various cells and tissues is required. Optimization of medium for a complex 3D bioprinted construct requires the consideration of all included cells and finding a balance between the different components required by each cell type (Vis, 2020; Zhu, 2018). Regarding the skin model, the optimized media should support the differentiation of pre-adipocyte cells as well as the proliferation and tubular formation of endothelial cells. In addition, the universal culture medium should provide the supplemental requirements for HDFs, melanocytes, and hair follicles. Therefore, universal culture medium for the 3D bioprinted construct was composed of 50% DMEM/F12 and 50% EGM-2 basal medium. Despite the positive role of IBMX on adipogenic differentiation of hAD-MSC, it was excluded from the universal culture medium due to its detrimental effect on HUVEC proliferation and vessel formation (Yang, 2020). In addition, hEGF was not used in the universal culture medium due to its inhibitory effect on adipogenic differentiation, although it is a great support for HUVEC proliferation (Yang, 2020). Insulin, T_3, dexamethasone, rosiglitazone and forskolin were added to the universal culture medium because of their pro-adipogenic properties (Yang, 2020). Based on the viability and morphology of the cells, the universal culture medium successfully met the requirements of the various cells included in the skin construct; it supported the formation of the vascularized hypodermis and dermis layers. However, further optimization of the bioprinting of hair follicles is needed.

Morphology

Histology staining was performed to evaluate the different layers of the 3D bioprinted skin construct at days 4, 7 and 14 post bioprinting **(Figure 3)**. The bright-field images of the epidermis layer indicated layer height varying from 20 µm to 150 µm **(Figure 3A, B, C)**, which is comparable to the lower values of native skin thickness (Oltulu, 2018). On the other hand, the epidermis layer was non-homogeneous, but this can be improved by optimizing the bioprinting settings for the EMD Printhead. The dermis layer for different samples were homogeneous, although few successfully bioprinted hair follicles **(Figure 3G)** could be observed. In upcoming studies, optimization of the 3D bioprinting process and bioink, as well as redesigning the construct, might improve the process of the 3D bioprinting of hair follicles. The lipid droplets of differentiated adipocytes in the hypodermis layer were identified with BODIPY493/503 and DAPI staining **(Figure 3I)**. Based on the bright-field images of the 3D bioprinted hypodermis layer, the average diameter of adipocytes cells was 10, 32 and 65 µm at days 4, 7 and 14, respectively **(Figure 3D, E, F)**. The adipocytes' enlargement over time is representative of a successful adipocyte maturation process post bioprinting.

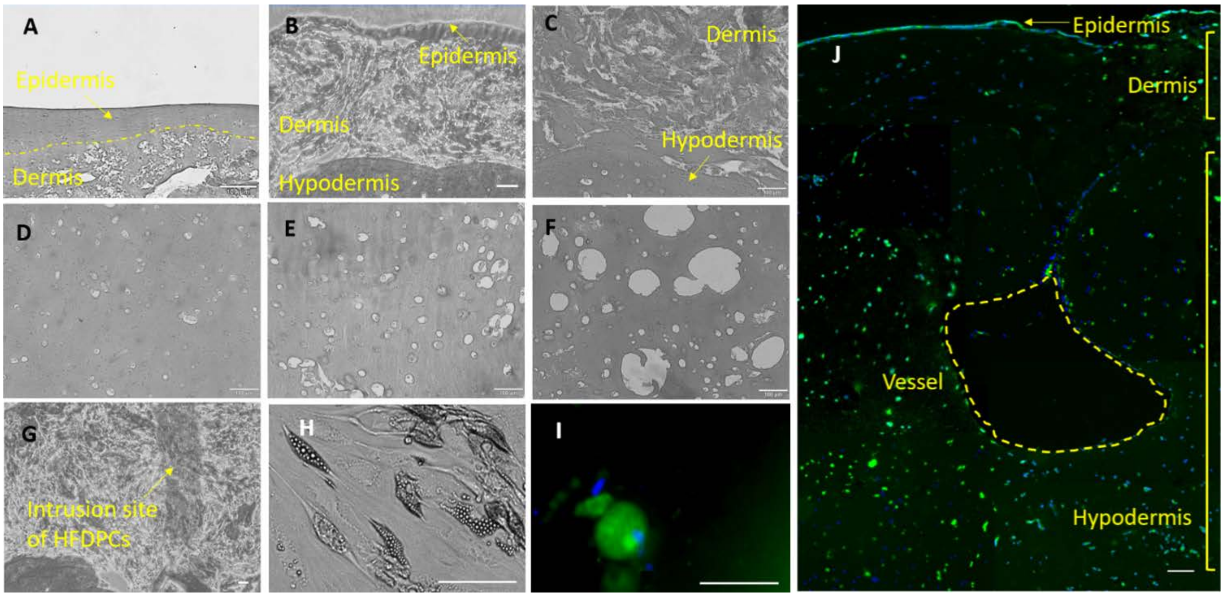

__Figure 3.__ Histology sections of the 3D bioprinted skin constructs post bioprinting. __A, B, C)__ Bright-field images of the skin construct at day 7 post bioprinting, __D)__ bright-field image of hypodermis at day 4, __E)__ bright-field image of hypodermis at day 7, __F)__ bright-field image of hypodermis 14 days post bioprinting, __G)__ intrusion demonstration of the HFDPCs in dermis layer, __H)__ bright-field image of the pre-adipocyte cells before bioprinting process, __I)__ lipid droplets of differentiated adipocytes in hypodermis layer at day 14 post bioprinting (BODIPY493/503 and DAPI staining), __J)__ immunofluorescence staining of actin in green and DAPI in blue, 14 days after bioprinting. Scale bars = 100 µm.

Conclusion

Development of a full-skin equivalent that contains all three layers of hypodermis, dermis and epidermis is highly valuable, not only for clinical applications but also as a complex skin model for pharmaceutical, cosmetic and toxicity testing. This study illustrates the 3D bioprinting capacity of CELLINK's BIO X6 bioprinter to fabricate a complex hierarchical skin tissue. It provides a robust platform for developing a complex hierarchical skin tissue, which includes epidermis, dermis, hypodermis, vessel and hair follicles. The universal culture medium, as well as GelMA FIBRIN bioink, successfully met the biological requirements for continued differentiation of the pre-adipocyte cells after bioprinting of the skin construct. The GelXA FIBRIN bioink, as well as the universal culture medium, provided a favorable environment for the development of the dermis layer. The BIO X6's coaxial bioprinting capabilities provided a great platform for bioprinting of the tubular structures of blood vessels in the skin model. The bioprinted skin construct highlighted the potential to mimic native skin anatomy. The BIO X6 facilitated the different bioprinting requirements for fabrication of a complex tissue design.

References

1. Boulais N, Pereira U, Lebonvallet N, Misery L. The whole epidermis as the forefront of the sensory system. *Experimental Dermatology*. 2007; 16(8): 634–635. DOI:10.1111/j.1600-0625.2007.00590.x.
2. Brohem CA, Cardeal LB, Tiago M, et al. Artificial skin in perspective: Concepts and applications. *Pigment Cell & Melanoma Research*. 2011; 24(1): 35–50. DOI:10.1111/j.1755-148X.2010.00786.x.
3. Centanni JM, Straseski JA, Wicks A, et al. StrataGraft skin substitute is well-tolerated and is not acutely immunogenic in patients with traumatic wounds: Results from a prospective, randomized, controlled dose escalation trial. *Annals of Surgery*. 2011; 253(4): 672–683. DOI:10.1097/SLA.0b013e318210f3bd.
4. Daikuara, LY, Chen X, Yue Z, et al. 3D bioprinting constructs to facilitate skin regeneration. *Advanced Functional Materials*. 2021; 32(3): 2105080. DOI:10.1002/adfm.202105080.
5. Douillet C, Nicodeme M, Hermant L, et al. From local to global matrix organization by fibroblasts: A 4D laser-assisted bioprinting approach. *Biofabrication*. 2022; 14(2): DOI:10.1088/1758-5090/ac40ed.
6. Gao G, Ahn M, Cho WW, et al. 3D printing of pharmaceutical application: drug screening and drug delivery. *Pharmaceutics*. 2021; 13(9): 1373. DOI:10.3390/pharmaceutics13091373.
7. Gauglitz GG, Korting HC, Pavicic T, et al. Hypertrophic scarring and keloids: Pathomechanisms and current and emerging treatment strategies. *Molecular Medicine*. 2011; 17(1-2): 113–125. DOI:10.2119/molmed.2009.00153.
8. Gilaberte Y, Prieto-Torres L, Pastushenko I, Juarranz Á. Anatomy and function of the skin. In: Hamblin MR, Avci P, Prow TW, eds. *Nanoscience in Dermatology*. Academic Press; 2016: 1–14. DOI:10.1016/B978-0-12-802926-8.00001-X.
9. Huber B, Link A, Linke K, et al. Integration of mature adipocytes to build-up a functional three-layered full-skin equivalent. *Tissue Engineering. Part C Methods*. 2016; 22(8): 756–764. DOI:10.1089/ten.TEC.2016.0141.
10. Javaid M, Haleem A. 3D bioprinting applications for the printing of skin: A brief study. *Sensors International*. 2021; 2: 100123. DOI:10.1016/j.sintl.2021.100123.
11. Lee VK, Lanzi AM, Haygan N, et al. Generation of multi-scale vascular network system within 3D hydrogel using 3D bio-printing technology. *Cellular and Molecular Bioengineering*. 2014; 7(3): 460–472. DOI:10.1007/s12195-014-0340-0.

12. Li L, Yu F, Shi J, et al. In situ repair of bone and cartilage defects using 3D scanning and 3D printing. *Scientific Reports*. 2017; 7(1): 9416. DOI:10.1038/s41598-017-10060-3.
13. Ma J, Wang Y, Liu J. Bioprinting of 3D tissues/organs combined with microfluidics. *RSC Advances*. 2018; 8(39): 21712–21727. DOI:10.1039/C8RA03022G.
14. Marston WA. Dermagraft, a bioengineered human dermal equivalent for the treatment of chronic nonhealing diabetic foot ulcer. *Expert Review of Medical Devices*. 2004; 1(1): 21–31. DOI:10.1586/17434440.1.1.21.
15. Martin P, Nunan R. Cellular and molecular mechanisms of repair in acute and chronic wound healing. *The British Journal of Dermatology*. 2015; 173(2): 370–378. DOI:10.1111/bjd.13954.
16. Miri AK, Mirzaee I, Hassan S, et al. Effective bioprinting resolution in tissue model fabrication. *Lab on a Chip*. 2019; 19(11): 2019–2037. DOI:10.1039/C8LC01037D.
17. Oltulu P, Ince B, Kokbudak N, et al. Measurement of epidermis, dermis, and total skin thicknesses from six different body regions with a new ethical histometric technique. *Turkish Journal of Plastic Surgery*. 2018; 26(2): 56–61. DOI:10.4103/tjps.TJPS_2_17.
18. Richters CD, Hoekstra MJ, du Pont JS, et al. Immunology of skin transplantation. *Clinics in Dermatology*. 2005; 23(4): 338–342. DOI:10.1016/j.clindermatol.2004.07.022.
19. Schneider J, Biedermann T, Widmer D, et al. Matriderm versus Integra: A comparative experimental study. *Burns*. 2009; 35(1): 51–57. DOI:10.1016/j.burns.2008.07.018.
20. Shevchenko RV, James SL, James SE. A review of tissue-engineered skin bioconstructs available for skin reconstruction. *Journal of the Royal Society Interface*. 2010; 7(43): 229–258. DOI:10.1098/rsif.2009.0403.
21. Starcher B, Aycock RL, Hill CH. Multiple roles for elastic fibers in the skin. *Journal of Histochemistry & Cytochemistry*. 2005; 53(4): 431–443. DOI:10.1369/jhc.4A6484.2005.
22. Thompson CM, Hocking AM, Honari S, et al. Genetic risk factors for hypertrophic scar development. *Journal of Burn Care & Research*. 2013; 34(5): 477–482. DOI:10.1097/BCR.0b013e3182a2aa41.
23. Vis MAM, Ito K, Hofmann S. Impact of culture medium on cellular interactions in in vitro co-culture systems. *Frontiers in Bioengineering and Biotechnology*. 2020; 8. DOI:10.3389/fbioe.2020.00911.
24. Weng T, Zhang W, Xia Y, et al. 3D bioprinting for skin tissue engineering: Current status and perspectives. *Journal of Tissue Engineering*. 2021; 12. DOI:10.1177/20417314211028574.
25. Widjaja W, Maitz P. The use of dermal regeneration template (Pelnac) in acute full-thickness wound closure: A case series. *European Journal of Plastic Surgery*. 2016; 39(2): 125–132. DOI:10.1007/s00238-015-1131-0.
26. Xu Y, Wang X. Fluid and cell behaviors along a 3D printed alginate/gelatin/fibrin channel. *Biotechnology and Bioengineering*. 2015; 112(8): 1683–1695. DOI:10.1002/bit.25579.
27. Yang F, Cohen RN, Brey EM. Optimization of co-culture conditions for a human vascularized adipose tissue model. *Bioengineering (Basel)*. 2020; 7(3): 114. DOI:10.3390/bioengineering7030114.
28. 28. Zhu S, Ehnert S, Rouß M, et al. From the clinical problem to the basic research: Co-culture models of osteoblasts and osteoclasts. *International Journal of Molecular Sciences*. 2018; 19(8): 2284. DOI:10.3390/ijms19082284.

CELLINK
A BICO COMPANY

FUTURE
LAB INNOVATIONS

For the BeNeLux and DACH-region, contact Future Lab Innovations

info@futurelabinnovations.com
www.futurelabinnovations.com

Read other application notes